Thermodynamics of Ni^{2+}, Cu^{2+}, and Zn^{2+} Binding to the Urease Metallochaperone UreE†

Nicholas E. Grossoehme,‡ Scott B. Mulrooney,§ Robert P. Hausinger,§,|| and Dean E. Wilcox*,‡

Department of Chemistry, Dartmouth College, Hanover, New Hampshire 03755, and Department of Microbiology and Molecular Genetics and Department of Biochemistry and Molecular Biology, Michigan State University, East Lansing, Michigan 48824

Received January 26, 2007; Revised Manuscript Received June 22, 2007

ABSTRACT: The two Ni^{2+} ions in the urease active site are delivered by the metallochaperone UreE, whose metal binding properties are central to the assembly of this metallocenter. Isothermal titration calorimetry (ITC) has been used to quantify the stoichiometry, affinity, and thermodynamics of Ni^{2+}, Cu^{2+}, and Zn^{2+} binding to the well-studied C-terminal truncated H144*UreE from *Klebsiella aerogenes*, Ni^{2+} binding to the wild-type *K. aerogenes* UreE protein, and Ni^{2+} and Zn^{2+} binding to the wild-type UreE protein from *Bacillus pasteurii*. The stoichiometries and affinities obtained by ITC are in good agreement with previous equilibrium dialysis results, after differences in pH and buffer competition are considered, but the concentration of H144*UreE was found to have a significant effect on metal binding stoichiometry. While two metal ions bind to the H144*UreE dimer at concentrations $<10\ \mu$M, three Ni^{2+} or Cu^{2+} ions bind to 25 μM dimeric protein with ITC data indicating sequential formation of Ni/Cu(H144*UreE)$_4$ and then (Ni/Cu)$_2$(H144*UreE)$_4$, or Ni/Cu(H144*UreE)$_2$, followed by the binding of four additional metal ions per tetramer, or two per dimer. The thermodynamics indicate that the latter two metal ions bind at sites corresponding to the two binding sites observed at lower protein concentrations. Ni^{2+} binding to UreE from *K. aerogenes* is an enthalpically favored process but an entropically driven process for the *B. pasteurii* protein, indicating chemically different Ni^{2+} coordination to the two proteins. A relatively small negative value of ΔC_p is associated with Ni^{2+} and Cu^{2+} binding to H144*UreE at low protein concentrations, consistent with binding to surface sites and small changes in the protein structure.

Many enzymes require one or more metal ions whose intrinsic chemistry is the basis for the catalytic reaction. Organisms, therefore, invest genetic and biochemical resources to ensure that metalloenzymes incorporate the correct metal ion into their active site. Proteins responsible for the transport and delivery of metal ions have been designated metallochaperones (*1*, *2*), and, in many cases, the mechanism for inserting the correct metal ion into a nascent metalloenzyme is still poorly understood.

Urease possesses two Ni^{2+} ions at its active site that hydrolyzes urea to ammonia and carbamate, an essential reaction for certain microorganisms and plants (*3*, *4*). Attempts to substitute other metal ions to produce active urease have met with little success (*5*), and active urease cannot be prepared from apoprotein by simple addition of Ni^{2+} ions (*6*), unless an active site Lys has been post-translationally carbamylated (*7*). The X-ray crystallographic structures of ureases from *Klebsiella aerogenes* (*8*, *9*), *Bacillus pasteurii* (*10*), and other organisms have revealed that the active site is deeply buried, thereby limiting substrate accessibility and sequestering the Ni^{2+} ions from chelators.

Analysis of the *K. aerogenes* urease genetics identified several proteins coded by the *ureDABCEFG* operon that are required for generating a mature active enzyme. In addition to the three urease subunits, corresponding to UreA, UreB, and UreC, four accessory proteins are needed for biosynthesis of the nickel metallocenter (*11*, *12*). Three of these, UreD, UreF, and UreG, form a complex with urease apoprotein (*13*), rendering it competent for activation, while the metallochaperone UreE delivers the Ni^{2+} ions (*14*).

UreE, which has a single conserved His residue (His-96 in the *K. aerogenes* protein), has been the subject of several studies of its metal binding properties. *K. aerogenes* UreE (*Ka*UreE),[1] which behaves as a dimer during purification (*14*), has a C-terminal sequence in which 10 of the last 15 residues are histidine. Equilibrium dialysis showed that this protein binds 6.05 ± 0.25 Ni^{2+} per dimer with an average experimental K_d of 10 μM. X-ray absorption studies, including X-ray absorption near edge and extended X-ray absorp-

† These studies were supported by National Institutes of Health Grant DK45686 (to R.P.H.).

* To whom correspondence should be addressed. Tel: 603-646-2874. Fax: (603) 646-3946. E-mail: Dean.E.Wilcox@Dartmouth.edu.

‡ Dartmouth College.

§ Department of Microbiology and Molecular Genetics, Michigan State University.

|| Department of Biochemistry and Molecular Biology, Michigan State University.

[1] Abbreviations: *Ka*UreE, the UreE accessory protein from *Klebsiella aerogenes*; H144*UreE, *Ka*UreE truncated at residue 144; *Bp*UreE, UreE from *Bacillus pasteurii*; EDTA, ethylenediaminetetraacetic acid; EXAFS, extended X-ray absorption fine structure; ITC, isothermal titration calorimetry; NMR, nuclear magnetic resonance; Tes, 2-[tris-(hydroxymethyl)methylamino]-1-ethanesulfonic acid; Tris, 2-amino-2-(hydroxymethyl)-1,3-propanediol.

10.1021/bi700171v CCC: $37.00
Published on Web 08/21/2007

tion fine structure (EXAFS) measurements, and magnetic circular dichroism data indicate approximately octahedral coordination of the Ni^{2+} ions to 3−5 His residues (*14*).

A truncated form of *Ka*UreE, denoted H144*UreE, that lacks the His-rich tail but is competent for urease activation *in vivo* (*15*) has been studied extensively. Equilibrium dialysis data for this dimeric protein showed that two Ni^{2+} ions bind per dimer, with experimental K_d values of 1.5 and 47 μM (*16*). Electronic absorption spectra, EXAFS data, and paramagnetically shifted ^{1}H nuclear magnetic resonance (NMR) measurements indicate that there are two His ligands for the 5−6 coordinate Ni^{2+} ions bound to the protein (*17*). Absorption, electron paramagnetic resonance, and EXAFS data indicate that Cu^{2+} ions bind to H144*UreE in a tetragonal geometry that includes two His ligands, but less tightly bound Cu^{2+} also has a Cys ligand, as verified by resonance Raman measurements and spectroscopic studies of the C79A mutant (*16*, *17*).

The C-terminal His-rich sequence is not present in the UreE from some organisms. The best studied of these is *B. pasteurii* UreE (*Bp*UreE), which has a C-terminus ending in His-Gln-His (*18*) and behaves as a dimer during purification (*19*). Equilibrium dialysis studies have shown that *Bp*UreE binds two Ni^{2+} ions with experimental K_d values of 1.4 and 25 μM (*20*), while EXAFS and paramagnetically shifted ^{1}H NMR measurements confirm His coordination (*19*, *20*).

X-ray crystallography of H144*UreE and *Bp*UreE has shown that each protein is a head-to-head dimer, with the monomer consisting of two domains, a metal binding Atx1-like domain and an Hsp40-like peptide-binding domain. The 2.5 Å resolution structure of H91A H144*UreE with Cu^{2+} soaked into the protein crystals revealed the binding sites for three metal ions, one at the dimer interface bridging the His-96 residues and one per monomer coordinated to His-110 and His-112 at the periphery (*21*). *Bp*UreE crystallizes as a dimer of dimers with a single Zn^{2+} coordinated to His-100 (equivalent to His-96 in *Ka*UreE) from all four monomers (*22*). Unfortunately, crystallization and crystallographic analysis of UreE with bound Ni^{2+} ions has not yet been reported.

In spite of the availability of these protein structures and spectroscopic data on Ni^{2+} and Cu^{2+} ions bound to UreE, there are still a number of questions about this protein and its role in delivering Ni^{2+} to urease apoprotein. To further characterize the coordination chemistry of UreE, isothermal titration calorimetry (ITC) was used to quantify the stoichiometry, affinity, and thermodynamics of Ni^{2+}, Cu^{2+}, and Zn^{2+} binding to H144*UreE, Ni^{2+} binding to *Ka*UreE, and Ni^{2+} and Zn^{2+} binding to *Bp*UreE. We find that, after accounting for differences in pH and buffer, the ITC results are consistent with previously determined stoichiometries and metal affinities. However, the thermodynamics of Ni^{2+} binding to *Ka*UreE and *Bp*UreE are significantly different, with predominantly enthalpically favored binding for the former and entropically favored binding for the latter.

EXPERIMENTAL PROCEDURES

All metals were the highest purity chloride salts available and used as received from either Fisher or Sigma. Tris (2-amino-2-(hydroxymethyl)-1,3-propanediol, 99% pure) was obtained from Fisher, while Tes (2-[tris(hydroxymethyl)-methylamino]-1-ethanesulfonic acid) and EDTA (ethylenediaminetetraacetic acid) were both >99% pure and obtained from Sigma.

*Ka*UreE and H144*UreE samples were purified from *Escherichia coli* C41(DE3) cells containing pETWT or pETH144*, respectively, as described previously (*14*, *15*). The pACT-BpEFGD construct used for *Bp*UreE expression in *Escherichia coli* C41(DE3) cells is described elsewhere (*23*); the protein was purified by standard chromatographic methods using Ni-nitrilotriacetic acid, Superdex-75, and Q-Sepharose resins (GE Healthcare). Protein concentrations were determined spectrophotometrically, based on molar extinction coefficients at 280 nm calculated from the protein sequences (*24*): 5120 M^{-1} cm^{-1} for H144*UreE and *Ka*UreE, and 21 430 M^{-1} cm^{-1} for *Bp*UreE.

ITC experiments were carried out at 25 ± 0.2 °C, unless indicated otherwise, on a MicroCal VP-ITC calorimeter, as described previously (*25*). Samples were buffered at pH 7.45 with either 100 mM Tris or 50 mM Tes, and the ionic strength was adjusted to 100 mM with NaCl. The concentrations of stock metal solutions were verified by ITC titrations against standardized EDTA solutions. A typical experiment consisted of a ~0.25 mM or ~1 mM metal solution titrated into an identically buffered ~7 μM dimeric protein solution. Two or, more typically, three good data sets were collected for each type of titration, and the best-fit values were averaged and reported. The ITC data are presented as the baseline-adjusted raw data in the top panel and the peak-integrated, concentration-normalized heat of reaction versus the molar ratio of metal ion to protein dimer (or tetramer, where noted) in the bottom panel.

The ITC data were fitted with the Origin software package provided by MicroCal (*26*), which uses a nonlinear least-squares algorithm (minimization of χ^2) and the concentrations of the titrant and the sample to fit the heat flow per injection to equations corresponding to an equilibrium binding model, providing best-fit values for the stoichiometry (n_{ITC}), change in enthalpy (ΔH_{ITC}), and binding constant (K_{ITC}). Three different binding models, which have different assumptions and number of fit parameters, were used in this fitting, the one site model (3 parameters), the two independent sites model (6 parameters), and the multiple sequential sites model (2 parameters per site). The latter model imposes a sequential filling of individual binding sites and fixes the stoichiometry of each site at 1. Comparison of the goodness of fit with different models was based on the calculated χ^2 value.

The best-fit ΔH_{ITC} values for experiments in two or more buffers were then used to quantify the number of protons that are displaced upon metal binding. This is described in detail elsewhere (*27*, *28*), and is based on the observation that the major difference between ΔH_{ITC} measured in two different buffers is due to the buffer protonation enthalpy (ΔH_{buffH+}) times the number of protons (n_{H+}) that are displaced; thus, a plot of ΔH_{ITC} versus ΔH_{buffH+} can be used to determine n_{H+} at the experimental pH.

Analysis of the experimental K_{ITC} (ΔG_{ITC}) and ΔH_{ITC} values for the overall titration equilibrium in a thermodynamic cycle, consisting of $\Delta G°$ and $\Delta H°$ values for individual relevant equilibria, was then used to determine the buffer- and pH-independent log K ($\Delta G°$) and $\Delta H°$ values for metals binding to the proteins, as described elsewhere

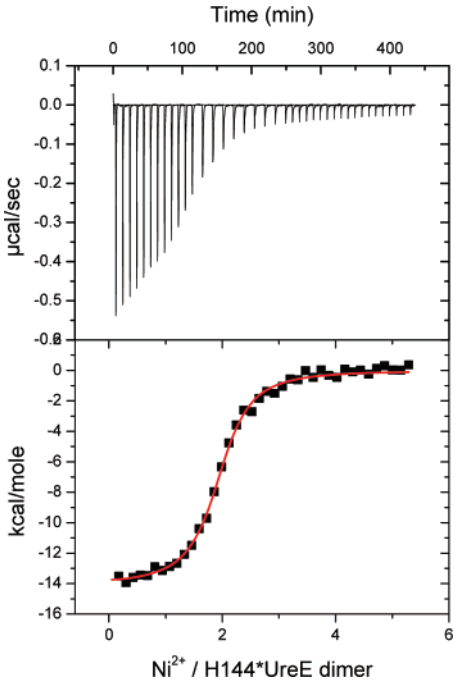

FIGURE 1: ITC data for the 25 °C titration of 0.25 mM Ni^{2+} into 6 μM H144*UreE dimer in 100 mM Tris, pH 7.45, and $I = 0.10$ M. The upper panel contains the baseline-corrected raw data, and the lower panel indicates the peak-integrated, concentration-normalized heats of reaction versus the molar ratio of Ni^{2+} per protein dimer. The solid line in the lower panel represents the best fit of the data using the one site model with $n_{ITC} = 1.92 \pm 0.01$, $K_{ITC} = 3.2 \pm 0.2 \times 10^6$, $\Delta H_{ITC} = -14.1 \pm 0.1$ kcal/mol.

(*26*, *27*). Finally, the thermodynamic relationship $\Delta G° = \Delta H° - T\Delta S°$ was used to find the entropic contribution to binding.

RESULTS AND ANALYSIS

*Ni^{2+} Binding to H144*UreE.* ITC was used to quantify Ni^{2+} binding to H144*UreE from *K. aerogenes*, and Figure 1 shows a representative thermogram of Ni^{2+} titrated into the protein at pH 7.45 in 100 mM Tris buffer. A good fit to these data can be achieved using the one site model in the Origin software provided with the MicroCal titration calorimeter, and the average best-fit experimental values (n_{ITC}, K_{ITC}, ΔH_{ITC}) in Tris and Tes buffers are summarized in Table 1. In agreement with previous results (*15*, *16*), the data clearly demonstrate that two (1.9 ± 0.1) Ni^{2+} ions bind to the protein dimer, but their affinities and enthalpies are indistinguishable by ITC, suggesting similar binding sites. Reverse titrations of H144*UreE into Ni^{2+} solutions (Figure S1 in Supporting Information) have an inflection at $n_{ITC} = 0.5$ and are well fitted with similar values.

Since ITC measures the total heat flow upon injection of titrant and titrations with metal ions typically have coupled equilibria involving the buffer and protonation, all of the equilibria that contribute to the experimental K_{ITC} and ΔH_{ITC} values need to be considered to determine $\Delta G°$ (K_d) and $\Delta H°$ for the equilibrium of interest (*25*). The two buffers were chosen not only for their buffering capacity at the desired pH but also for their formation of well-defined metal−buffer complexes (Table S1 in Supporting Information) that prevent metal hydrolysis reactions and allow the metal−buffer interactions to be accurately subtracted from K_{ITC} and ΔH_{ITC}. In addition, metal ions often displace protons when they bind to protein residues, and this leads to buffer protonation, which is another contribution to both K_{ITC} and ΔH_{ITC}. To account for these coupled protonation equilibria, the number of protons that are transferred at the experimental pH needs to be determined. As described in detail elsewhere (*27*, *28*), the number of displaced protons can be quantified through an analysis of the experimental enthalpies (ΔH_{ITC}) for two or more ITC titrations at the same pH with different buffers, and thus different buffer protonation enthalpies. Such an analysis of these ITC data in Tris and Tes buffers indicates that 0.90 proton is displaced when each Ni^{2+} binds to H144*UreE at pH 7.45.

To extract the thermodynamic parameters ($\Delta G°$, $\Delta H°$, $\Delta S°$) for metal ion binding to proteins from the experimental ITC parameters, thermodynamic cycles were constructed for an analysis of the overall reaction that occurs upon addition of titrant. An example is shown in eqs 1−6 for Ni^{2+} binding to a H144*UreE subunit in Tris buffer, which is an appropriate cycle for Ni^{2+} binding to isolated sites on the subunits of the UreE dimer.

$$x\mathrm{NiTris}^{2+} + y\mathrm{Ni(Tris)_2}^{2+} + (1-x-y)\mathrm{Ni}^{2+} + (1-r)\text{H144*UreE} + r\text{H144*UreE-H}^{+} + (r-x-2y)\mathrm{Tris} \rightleftharpoons \text{H144*UreE-Ni}^{2+} + r\mathrm{TrisH}^{+} \quad (1)$$

$$x\{\mathrm{NiTris}^{2+} \rightleftharpoons \mathrm{Ni}^{2+} + \mathrm{Tris}\} \quad (2)$$

$$y\{\mathrm{Ni(Tris)_2}^{2+} \rightleftharpoons \mathrm{Ni}^{2+} + 2\mathrm{Tris}\} \quad (3)$$

$$r\{\text{H144*UreE-H}^{+} \rightleftharpoons \text{H144*UreE} + \mathrm{H}^{+}\} \quad (4)$$

$$\mathrm{Ni}^{2+} + \text{H144*UreE} \rightleftharpoons \text{H144*UreE-Ni}^{2+} \quad (5)$$

$$r\{\mathrm{H}^{+} + \mathrm{Tris} \rightleftharpoons \mathrm{TrisH}^{+}\} \quad (6)$$

The overall reaction for the formation of H144*UreE-Ni^{2+} is given by eq 1, where $x = 0.35$, $y = 0.60$, and $r = 0.90$ are coefficients that are fixed by the experimental conditions (pH 7.45, 100 mM Tris) and indicate the different Ni^{2+} species (60% $Ni(Tris)_2^{2+}$, 35% $NiTris^{2+}$, 5% Ni^{2+}) and the H144*UreE protonation states relevant to the Ni^{2+} binding reaction (90% H144*UreE-H^+, 10% H144*UreE) that are present in solution. The cycle is then constructed from the relevant weighted individual equilibria (eqs 2−6) that sum to the overall equilibrium (eq 1) and allow the buffer- and pH-independent values of $\Delta G°$ (K) and $\Delta H°$ for Ni^{2+} binding to the protein (eq 5) to be determined (e.g., $\Delta H_{ITC} = x\Delta H°_{eq2} + y\Delta H°_{eq3} + r\Delta H°_{eq4} + \Delta H°_{eq5} + r\Delta H°_{eq6}$). Pertinent $\Delta G°$ (K_1, β_2) and $\Delta H°$ values for metal−buffer interaction (e.g., eqs 2, 3), including several determined as part of this study, are found in Table S1 (Supporting Information). Other necessary values are those associated with the 0.90 proton that Ni^{2+} displaces upon binding to the protein (eq 4) and the subsequent buffer protonation (eq 6), for which pK_a and $\Delta H°$ values are known. Since NMR and EXAFS data indicate that each bound Ni^{2+} has two His ligands, the displaced 0.90 proton is likely to be associated with these residues and eq 4 was modeled[2] with $pK_a = 8.40$ and the His deprotonation enthalpy (7.10 kcal/mol (*29*)).

Analogous thermodynamic cycles that include $\Delta G°$ and $\Delta H°$ values for the relevant metal−buffer species and protein protonation states under the experimental conditions were

Table 1: Summary of Average Best-Fit Values[a] from 25 °C ITC Data for UreE Dimer Titrations, the Corresponding pH- and Buffer-Independent Values, and Idealized Total Metal−Dimer Ratios.

	protein	buffer	n_{ITC}[b]	K_{ITC}	ΔH_{ITC} (kcal/mol)	log K	$\Delta H°$ (kcal/mol)	total M^{2+}/dimer
Ni^{2+}	H144*UreE[c]	Tris	1.9 (0.1)	$2.8 \pm 0.4 \times 10^6$	−14.1 (0.2)	8.8 (0.2)	−14 (2)	2
		Tes	2.2 (0.1)	$2.6 \pm 0.3 \times 10^6$	−14.9 (0.1)	8.8 (0.1)	−14 (4)	2
	KaUreE[d]	Tris	2	$1.0 \pm 0.5 \times 10^6$	−13.3 (0.8)			2
			3.3 (0.2)	$1.0 \pm 0.1 \times 10^5$	−5.8 (0.5)	6.98 (0.08)	−5 (2)	5−6
		Tes	2	$1.7 \pm 0.7 \times 10^6$	−13.3 (0.4)			2
			3.1 (0.4)	$7 \pm 1 \times 10^4$	−5 (1)	6.89 (0.09)	−5 (3)	5−6
	*Bp*UreE[e]	Tris	1	$1.3 \pm 0.4 \times 10^5$	−3.3 (0.4)	7.55 (0.08)	−3 (1)	1
			1	$3 \pm 1 \times 10^3$	−2 (3)	6.2 (0.2)	0 (4)	2
		Tes	1	$1.2 \pm 0.4 \times 10^5$	−3.2 (0.5)	7.5 (0.2)	−2 (1)	1
			1	$1.6 \pm 0.7 \times 10^4$	−1 (1)	6.7 (0.2)	2 (2)	2
Cu^{2+}	H144*UreE[c]	Tris	2.1 (0.1)	$4.5 \pm 0.2 \times 10^5$	−9.2 (0.1)	10.8 (0.5)	−10 (4)	2
		Tes	2.2 (0.1)	$1.2 \pm 0.1 \times 10^6$	−9.6 (0.1)	11.3 (0.2)	−10 (4)	2
Zn^{2+}	H144*UreE[c]	Tris	2.2 (0.1)	$1.3 \pm 0.1 \times 10^5$	−11.7 (0.3)	7.06 (0.08)	−11 (2)	2
	BpUreE[f]	Tris		$9.8 \pm 0.7 \times 10^3$				

[a] Values are from fits with the one site model, unless indicated otherwise; the associated error is shown in parentheses. [b] Integer value is a fixed fit parameter. [c] Values for H144*UreE were obtained with low protein dimer concentrations (<10 μM). [d] Best fits were obtained with the two independent sites model. [e] Best fits were obtained with the two sequential sites model, which imposes a stoichiometry of 1 for each site. [f] Average of fits using a one site model with $n_{ITC} = 1$ and $n_{ITC} = 2$.

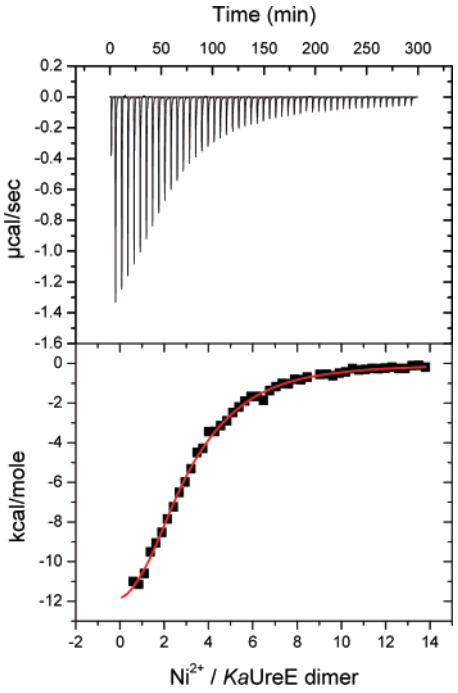

FIGURE 2: ITC data for the 25 °C titration of 0.63 mM Ni^{2+} into 10 μM *Ka*UreE dimer in 100 mM Tris, pH 7.45, and $I = 0.10$ M. The solid line is the best fit of the data using the two independent sites model with $n_{1,ITC} = 2$ (fixed), $K_{1,ITC} = 1.0 \pm 0.4 \times 10^6$, $\Delta H_{1,ITC} = -13.4 \pm 0.7$ kcal/mol, $n_{2,ITC} = 3.2 \pm 0.3$, $K_{2,ITC} = 1.0 \pm 0.2 \times 10^5$, $\Delta H_{2,ITC} = -5.5 \pm 0.8$ kcal/mol.

used to analyze the best-fit experimental ITC data for metal ions binding to the proteins. The buffer- and pH-independent thermodynamic values (log K, $\Delta H°$) for equilibria corresponding to eq 5 that were determined from these analyses are found in Table 1.

Ni^{2+} Binding to Full-Length KaUreE. The ITC data for Ni^{2+} binding to full length *Ka*UreE (Figure 2) are qualitatively different than data for the truncated protein. Notably, the reaction continues to higher Ni^{2+}/dimer ratios, as expected from the presence of the additional His residues. In the absence of clear inflection points, several models were evaluated for fitting these experimental data. While a reasonable fit ($\chi^2 = 7.05 \times 10^4$) can be achieved with the one site model ($n_{ITC} = 3.0 \pm 0.1$, $K_{ITC} = 1.3 \pm 0.1 \times 10^5$, $\Delta H_{ITC} = -15.1 \pm 0.3$ kcal/mol), where all Ni^{2+} ions bind to equivalent sites, the stoichiometry is significantly lower than that determined previously by equilibrium dialysis (*14*). Assuming that the C-terminal 15 residues bind *additional* Ni^{2+} ions more weakly than the rest of the protein dimer binds the first two Ni^{2+} ions, the data were fit using the two independent sites model and fixing the stoichiometry of the first type of site ($n_{1,ITC}$) at 2. The better fit ($\chi^2 = 2.14 \times 10^4$) with this model gives $K_{1,ITC}$ and $\Delta H_{1,ITC}$ values in Tris and Tes (Table 1) for the first type of site that are very similar to those determined for H144*UreE under identical conditions, supporting the use of this model and indicating analogous binding thermodynamics for the first two Ni^{2+} ions that bind to both the full length and the C-terminal truncated *Ka*UreE dimer.

The best-fit values for the second type of site indicate average values for the additional Ni^{2+} ions that bind to the His-rich tail. Of particular interest is the value $n_{2,ITC} = 3.3 \pm 0.2$ in Tris (3.1 ± 0.4 in Tes), resulting in 5.3 (5.1 in Tes) total Ni^{2+} ions that bind to the *Ka*UreE dimer, which is close to the value determined by equilibrium dialysis (*14*). Further, preliminary ITC data with a 15 residue peptide corresponding to the *Ka*UreE C-terminal sequence indicate a binding stoichiometry of 1.7 Ni^{2+}, which corresponds to 3.4 Ni^{2+} per peptide dimer (J. Cui, N. E. Grossoehme, D. E. Wilcox, unpublished results). As above, analysis of $\Delta H_{2,ITC}$, which includes the binding enthalpy for these additional Ni^{2+} ions, in the two buffers indicates the displacement of 1.23 protons per Ni^{2+} at pH 7.45. Based on *Ka*UreE EXAFS data, which showed that Ni^{2+} ions coordinate to 3−5 His residues, this contribution to the thermodynamic analysis was again modeled[2] with the His deprotonation enthalpy and four His pK_a values of 6.5, 6.9, 7.3, and 7.7. Analysis with the relevant thermodynamic cycles in Tris and Tes buffers led to the buffer- and pH-independent results in Table 1.

[2] Since the only experimental parameter is the number of displaced protons, the pK_as were chosen to give the experimentally determined protonation state at pH 7.45. While many combinations of pK_as achieve this goal, different choices have little impact on the buffer- and pH-independent free energy values. The choice of protonation enthalpy, however, has a larger effect on the calculated value for the binding enthalpy.

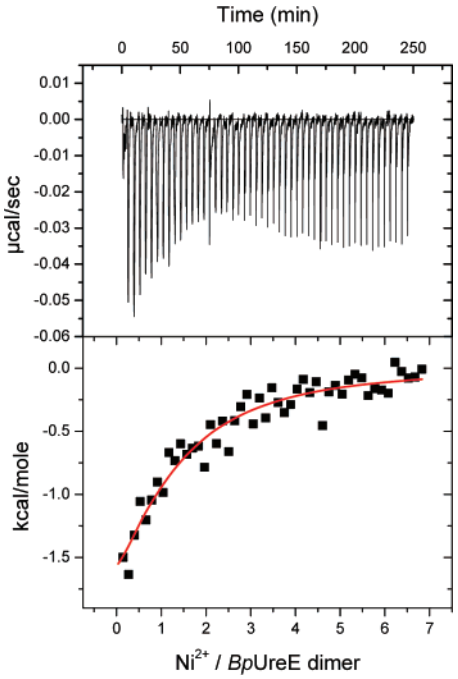

FIGURE 3: ITC data for the 25 °C titration of 0.25 mM Ni^{2+} into 8.4 μM *Bp*UreE dimer in 50 mM Tes, pH 7.45, and $I = 0.10$ M. The solid line is the best fit of the data using the two sequential sites model with $K_{1,ITC} = 1.2 \pm 0.5 \times 10^6$, $\Delta H_{1,ITC} = -3.2 \pm 0.7$ kcal/mol, $K_{2,ITC} = 2 \pm 1 \times 10^4$, $\Delta H_{2,ITC} = -1 \pm 1$ kcal/mol.

Ni^{2+} Binding to BpUreE. Representative ITC data for Ni^{2+} binding to *Bp*UreE are shown in Figure 3. Significantly less heat is produced than with Ni^{2+} binding to *Ka*UreE, but the titration profile indicates that approximately two Ni^{2+} ions bind to the dimer, in agreement with a recent report (*20*). Reasonable fits can be achieved with the one site model and n_{ITC} either floating or fixed at 2, but these fits give low values for K_{ITC}. Better fits of the ITC data in both Tris and Tes buffers were obtained with the two sequential sites model, which gives larger $K_{1,ITC}$ and $K_{2,ITC}$ values that differ by 1−2 orders of magnitude (Table 1). Proton displacement upon Ni^{2+} coordination at pH 7.45 was determined from an analysis of $\Delta H_{1,ITC}$ and $\Delta H_{2,ITC}$, as indicated above, to be 1.1 ± 0.2 and 1.5 ± 0.9 for the first and second sites, respectively, with the larger error for the latter resulting from the low experimental heat and, therefore, a low signal-to-noise ratio. Analyzing the overall experimental reaction in Tris and Tes in thermodynamic cycles, like that in eqs 1−6, which account for the Ni^{2+}-displaced protons by elevated His pK_as and the His protonation enthalpy, as before, leads to the buffer- and pH-independent values in Table 1.

*Cu^{2+} Binding to H144*UreE.* The ITC data for Cu^{2+} binding to H144*UreE at a dimer concentration of 6 μM (Figure 4A) indicate that two ions bind to the protein with indistinguishable parameters, and average best-fit values using the one site model are found in Table 1. Since Cu^{2+} forms a very stable complex with Tris ($Cu(Tris)_4^{2+}$, log $\beta_4 = 14.1$ (*29*)) but a much weaker complex with Tes ($Cu(Tes)^{2+}$, log $K_1 = 3.90$ (*30*)) and the complexes have different enthalpies of formation (Table S1 in Supporting Information), it was somewhat surprising that the *experimental* binding constant (K_{ITC}) and reaction enthalpy (ΔH_{ITC}) in the two buffers were not significantly different. Using the free energy and enthalpy of formation of $Cu(Tris)_4^{2+}$ (i.e., an equilibrium corresponding to eq 3 for $Cu(Tris)_4^{2+}$) in the analysis of ΔH_{ITC} to determine the number of protons that each Cu^{2+} displaces gives a value of 3.4, which is incommensurate with the 0.90 proton displaced by Ni^{2+}. Further, analysis with a thermodynamic cycle, like that in eqs 1−6, that includes loss of all four Tris ligands results in a buffer- and pH-independent Cu^{2+} binding constant of 2.4×10^{13}, which is 2 orders of magnitude larger than the value determined by a similar analysis of the data in Tes buffer. However, if it is assumed that each Cu^{2+} retains two Tris ligands when it binds to H144*UreE, as is possible with only two protein His ligands, then it is found that 0.93 proton is displaced, in good agreement with Ni^{2+} binding, and, more importantly, the thermodynamic analysis gives similar buffer- and pH-independent values for Cu^{2+} data obtained in either Tris or Tes buffers (Table 1).

Although ~7 μM H144*UreE provides ITC data with a good signal-to-noise ratio and results that are well within the *c*-window (*31*), at somewhat higher concentrations, or lower temperature, there is evidence of exothermic events occurring early in the Ni^{2+} and Cu^{2+} titrations when the protein is in excess (Figure S2 in Supporting Information). This prompted us to take measurements at higher protein concentrations, which give results that are qualitatively and quantitatively different. While Figure 4A shows the ITC data for a Cu^{2+} titration into 6 μM H144*UreE dimer, Figure 4B shows representative data for a titration under *identical* conditions with a 25 μM dimer sample. Three distinguishable events at Cu^{2+}-to-protein dimer ratios of 0.5, 1, and 3 are now clearly observed. The events at ratios of 1 and 3 are associated with the binding of one and then two more Cu^{2+} per dimer; however, the event at $n_{ITC} = 0.5$ indicates formation of a $Cu(H144*UreE)_4$ complex at this protein concentration, and required a different approach to fitting these data. Analogous Ni^{2+} titrations (Figure S3 in Supporting Information) are qualitatively similar.

These data were analyzed with two different approaches. In the first, the data were divided into two sets, one containing the events at molar ratios of 0.5 and 1 and the other encompassing the event at a molar ratio of 3, and the two data sets were fitted with the two independent sites and one site models, respectively. In the second approach, the analysis considered the number of metal ions per tetramer, so that inflections occur at molar ratios of 1, 2, and 6, and the data were fitted with the sequential sites model, which requires integer values of *n*. Average best-fit values with the two approaches (designated independent and sequential) for data obtained by titrating Ni^{2+} and Cu^{2+} into H144*UreE at the higher protein concentration are summarized in Table 2, where they are compared to average best-fit values at the lower protein concentration. The two metals that bind at the low protein concentration are designated as binding to "periphery" sites, while the metals binding at the high protein concentration are designated as "complex" at $n = 0.5$, "interface" at $n = 1$, and "periphery" for the final two metal ions. A striking fit of the whole thermogram for Cu^{2+}, or Ni^{2+}, binding per protein tetramer was achieved with the sequential sites model (Figure 4B, red line) and six sequential sites, with the constraint that the last four have identical K_{ITC} and ΔH_{ITC} values.

*Zn^{2+} Binding to H144*UreE and BpUreE.* Based on the previously reported Zn^{2+} competition with Ni^{2+} for binding

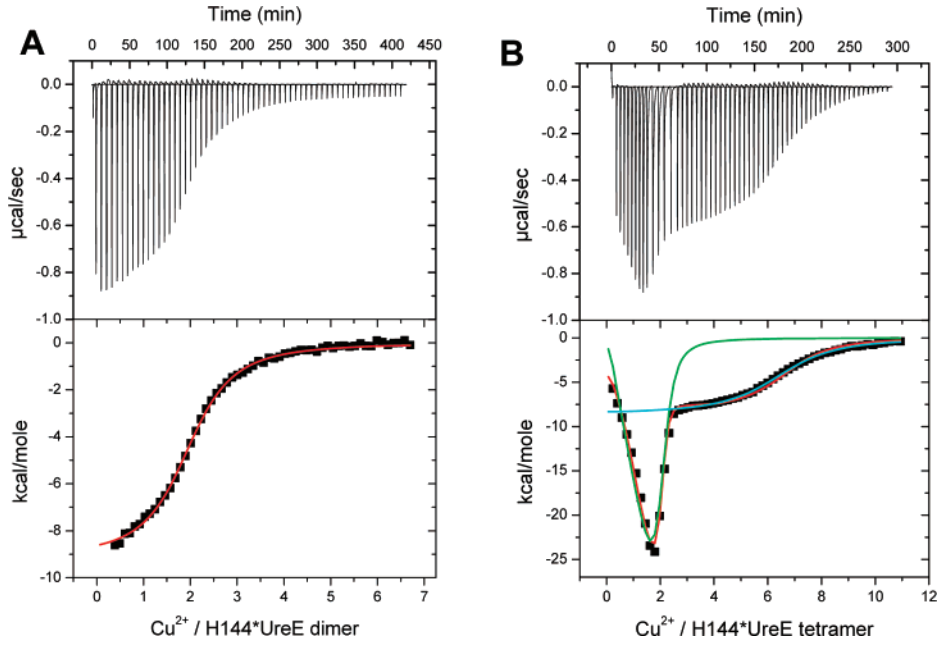

FIGURE 4: ITC data for the 25 °C titration of 0.40 mM Cu^{2+} into H144*UreE in 100 mM Tris, pH 7.45, and $I = 0.10$ M. (A) 6 μM dimer concentration. The solid red line is the best fit of the data using the one site model with $n_{ITC} = 2.02 \pm 0.01$, $K_{ITC} = 4.3 \pm 0.2 \times 10^5$, $\Delta H_{ITC} = -9.2 \pm 0.1$ kcal/mol. (B) 25 μM dimer concentration (note, abscissa is scaled per tetramer). The solid red line is the best fit with the sequential approach, while the blue and green lines are the best fit of the periphery sites and complex/interface sites, respectively, using the independent approach (see text for descriptions of the sites).

Table 2: Summary of Average Best-Fit Values[a] from 25 °C ITC Data for Titrations of Ni^{2+} and Cu^{2+} into H144*UreE in 100 mM Tris, pH 7.45 and Idealized Total Metal−Dimer Ratios

	Protein Concentration[b]	Site[c]	n_{ITC}[d]	K_{ITC}	ΔH_{ITC} (kcal/mol)	Total M^{2+}/dimer
Ni^{2+}	Low	*Periphery*	*1.9 (0.1)*	*2.8 ± 0.4 x10⁶*	*-14.1 (0.2)*	*2*
	High *Independent*	Complex	0.5	5 ± 14 x10⁶	-15.4 (0.8)	0.5
		Interface	0.5	7 ± 18 x10⁴	-44 (59)	1
		Periphery	*3.0 (0.1)*	*5.5 ± 0.6* x10⁶	*-14.24 (0.01)*	*3*
	High *Sequential*[e]	Complex	1	3 ± 1 x10⁸	-11(1)	0.5
		Interface	1	10 ± 2 x10⁷	-27 (1)	1
		Periphery	*4 × 1*	*1.2 ± 0.2* x10⁶	*-14 (2)*	*3*
Cu^{2+}	Low	*Periphery*	*2.1 (0.1)*	*4.5 ± 0.2 x10⁵*	*-9.2 (0.1)*	*2*
	High *Independent*	Complex	0.5	1.1 ± 0.6 x10⁷	-0 (4)	0.5
		Interface	0.5	3 ± 2 x10⁶	-36 (3)	1
		Periphery	*3.1 (0.1)*	*3.5 ± 0.1* x10⁵	*-9.18 (.08)*	*3*
	High *Sequential*[e]	Complex	1	2 ± 50 x10⁶	-4.2 (0.5)	0.5
		Interface	1	2.2 ± 0.5 x10⁷	-28.3 (0.7)	1
		Periphery	*4 × 1*	*2 ± 1* x10⁵	*-9 (8)*	*3*

[a] The associated error is shown in parentheses. Color of the data for the site corresponds to the color of the corresponding best-fit line for the Cu^{2+} titration data in Figure 4B. [b] The low concentration is <10 μM, and the high concentration is ~25 μM. [c] See text for description of the sites. [d] Integer or half-integer value is a fixed fit parameter. [e] Sequential model imposes a stoichiometry of 1; see text and Figure 4 for further description of the fitting procedure.

to H144*UreE (*15*), and chemical (*20*) and structural (*22*) results for Zn^{2+} interaction with *Bp*UreE, Zn^{2+} binding to these two proteins was studied by ITC. As found for Ni^{2+} and Cu^{2+}, two Zn^{2+} ions bind to ~6 μM H144*UreE dimer with indistinguishable parameters, and the fitting and analysis of these data exactly paralleled that of the Ni^{2+} and Cu^{2+} data at low protein concentrations, with the relevant thermodynamic data summarized in Table 1.

The titration of Zn^{2+} into *Bp*UreE (Figure S4, Supporting Information), however, produces very little heat, as observed for Ni^{2+} binding to this protein (Figure 3), and the enthalpy profile cannot be fit unambiguously. Best fits with a variety of models resulted in similar χ^2 values but quite different values of ΔH_{ITC}. However, similar K_{ITC} values were found with all one-site fits, regardless of n_{ITC} or ΔH_{ITC}, and the K_{ITC} value reported in Table 1 is an average of the best-fit values using the one-site model with $n_{ITC} = 1$ and $n_{ITC} = 2$.

Temperature Dependence of Metal Binding. The temperature dependence of Ni^{2+} and Cu^{2+} binding to H144*UreE at the low dimer concentration was determined. Identical ITC experiments were carried out at each temperature, and the temperature dependence of $\Delta H°$ and $\Delta G°$ for each reaction of the relevant thermodynamic cycle was determined from van't Hoff analysis or ΔC_p values that were calculated from published thermodynamic quantities (*29*) or results from this study (Table S2, Supporting Information). Table 3 reports

Table 3: Average Best-Fit Values[a] from ITC Data Using a One Site Model and Corresponding Buffer- and pH-Independent Values for Titrations of Ni^{2+} and Cu^{2+} into H144*UreE Dimer (6−7 μM) in 100 mM Tris, pH 7.45, at the Indicated Temperature

	°C	n_{ITC}	K_{ITC}	ΔH_{ITC} (kcal/mol)	log K	$\Delta H°$ (kcal/mol)
Ni^{2+}	10	1.9 (0.1)	$2.7 \pm 0.6 \times 10^6$	−14.2 (0.3)	9.0 (0.2)	−15 (2)
	25	1.9 (0.1)	$2.8 \pm 0.4 \times 10^6$	−14.1 (0.2)	8.8 (0.2)	−14 (2)
	37	1.9 (0.1)	$1.7 \pm 0.2 \times 10^6$	−15.1 (0.3)	8.4 (0.2)	−15 (3)
Cu^{2+}	10	2.0 (0.1)	$1.8 \pm 0.2 \times 10^6$	−8.2 (0.2)	11.7 (0.4)	−10 (2)
	25	2.1 (0.1)	$4.5 \pm 0.2 \times 10^5$	−9.2 (0.1)	10.8 (0.5)	−10 (4)
	37	2.1 (0.1)	$4.3 \pm 0.5 \times 10^5$	−10.3 (0.3)	10.5 (0.5)	−11 (2)

[a] The associated error is shown in parentheses.

the best-fit ITC values for these data, as well as the buffer- and pH-independent values. The resulting ΔC_p values for Ni^{2+} and Cu^{2+} binding to H144*UreE, as determined from the relationship $\Delta C_p = \partial \Delta H / \partial T$, are -30 ± 110 and -68 ± 120 cal/(mol K), respectively.

DISCUSSION

The mechanisms by which metal ions are post-translationally inserted into metalloproteins are poorly understood. One case that has been studied extensively is the Ni-containing enzyme urease, which requires four accessory proteins to generate its dinuclear Ni^{2+} metallocenter (*32*). Nevertheless, key information is still needed to understand this process, and this includes quantifying the coordination chemistry of the metallochaperone UreE that delivers Ni^{2+} ions to urease apoprotein. Since Ni^{2+} binding to, and release from, UreE is central to any urease activation mechanism, we have studied this and related metal binding equilibria.

Stoichiometry. The stoichiometry of metal ion coordination to *Ka*UreE, its H144*UreE truncated form, and *Bp*UreE have been quantified with ITC (Tables 1 and 2). As measured at low protein concentrations (<10 μM), H144*UreE binds two Ni^{2+}, Cu^{2+}, or Zn^{2+} ions per protein dimer with indistinguishable affinities at the two sites, the full length *Ka*UreE dimer binds a total of 5.0−5.5 Ni^{2+} ions, and the *Bp*UreE dimer binds two Ni^{2+} ions or a small (1−2), but poorly quantified, number of Zn^{2+} ions. These results are in agreement with previously determined stoichiometries for each protein (*14*−*16*, *20*).

Two observations motivated us to carry out ITC studies under different conditions. First, in contrast to crystallographic evidence that H144*UreE binds three Cu^{2+} per dimer (*21*), ITC data did not indicate binding events beyond $n_{ITC} = 2$ under the initial conditions. Second, titrations of Cu^{2+} into H144*UreE at somewhat higher concentrations, or at lower temperature, had initial injections that were significantly more exothermic than subsequent events, which suggested that the protein has additional exothermic metal binding equilibria when it is present at higher concentrations. Therefore, ITC measurements were carried out at a higher protein concentration (25 μM), at which H144*UreE exhibits dramatically different Ni^{2+} and Cu^{2+} binding isotherms, as seen in Figure 4B and Figure S3 (Supporting Information). In these titrations there is evidence for a tetramer complex (dimer of dimers) binding one metal and then a second metal (total of one per dimer), and then four additional metals (two more per dimer), with the final species containing three metals for each UreE dimer (Figure 5), in agreement with the stoichiometry of the X-ray structure of H91A H144*UreE crystals soaked with Cu^{2+} (*21*).

Careful examination of the ITC data reveals a connection between the lower and higher concentration titrations. Thermograms of Cu^{2+} titrated into the higher protein concentration (Figure 4B) have injections with a small endothermic feature subsequent to the major exothermic peak, but *only* after the $n_{ITC} = 1$ inflection and before the $n_{ITC} = 3$ inflection; similar endothermic features are observed in thermograms at the lower protein concentration for all peaks up to the $n_{ITC} = 2$ inflection (Figure 4A). These similar injection shapes suggest analogous chemical events and, in conjunction with similar values of K_{ITC} and ΔH_{ITC} for the periphery sites (Table 2), indicate that the two Cu^{2+}, or Ni^{2+}, ions that bind to the H144*UreE dimer at lower concentration correspond to the second and third metal ions that bind to the dimer at higher protein concentrations.

Metal binding to the dimer interface site or stabilization of a tetramer complex is not observed at lower protein concentrations, indicating a balance between the thermodynamics of protein−protein interaction and metal coordination, which may have functional relevance. Although we can estimate the concentration of H144*UreE in the recombinant overexpressing *E. coli* cells (~200 μM), the concentration of this protein in native *K. aerogenes* cells is expected to be much lower and may vary with factors that control expression of the *ure* operon. Thus, it is not known if the dimer, which is the UreE form that is observed during chromatographic purification in the absence or presence of Ni^{2+}, or the tetrameric form of UreE predominates in the cell. However, the tetramer may mimic the situation when a UreE dimer interacts with the protein complex containing urease apoprotein. This interaction may favor Ni^{2+} migration from the periphery sites to sites that are analogous to the complex and interface sites involving the essential His-96, followed by transfer into urease.

These results are substantially consistent with previous data on both H144*UreE and *Bp*UreE. The higher protein concentration is closer to that used for crystallization, and H144*UreE crystals soaked with Cu^{2+} ions revealed a metal bound to both His-96 residues at the dimer interface, as well as one bound to each pair of His-110 and His-112 residues on the periphery of each monomer (*21*). Although there are no reports of a tetrameric structure for *Ka*UreE, and no direct evidence was found here, this has been reported for Ni^{2+} binding to *Bp*UreE at millimolar concentrations (*33*) and is seen in the *Bp*UreE crystal structure, with a Zn^{2+} coordinated to the four His-100 residues (equivalent to His-96 in *Ka*UreE) that lie in close proximity (*22*).

Binding Constants. Quantitative comparison of binding (dissociation) constants determined by ITC to those determined by equilibrium dialysis requires that any difference in pH and buffer competition for the metal ions be removed. For example, K_d values for Ni^{2+} binding to H144*UreE have been determined by equilibrium dialysis in 50 mM phosphate at pH 7.2 with 85 mM NaCl (*15*) and in 20 mM Tris at pH 7.5 with 100 mM NaCl (*16*), while the ITC measurements have been made in 100 mM Tris at pH 7.45 with $I = 0.10$ M. Table 1 includes the buffer- and pH-independent binding constants obtained from the ITC data, and we have similarly accounted for metal−buffer interaction and proton competition associated with K_d values reported from equilibrium

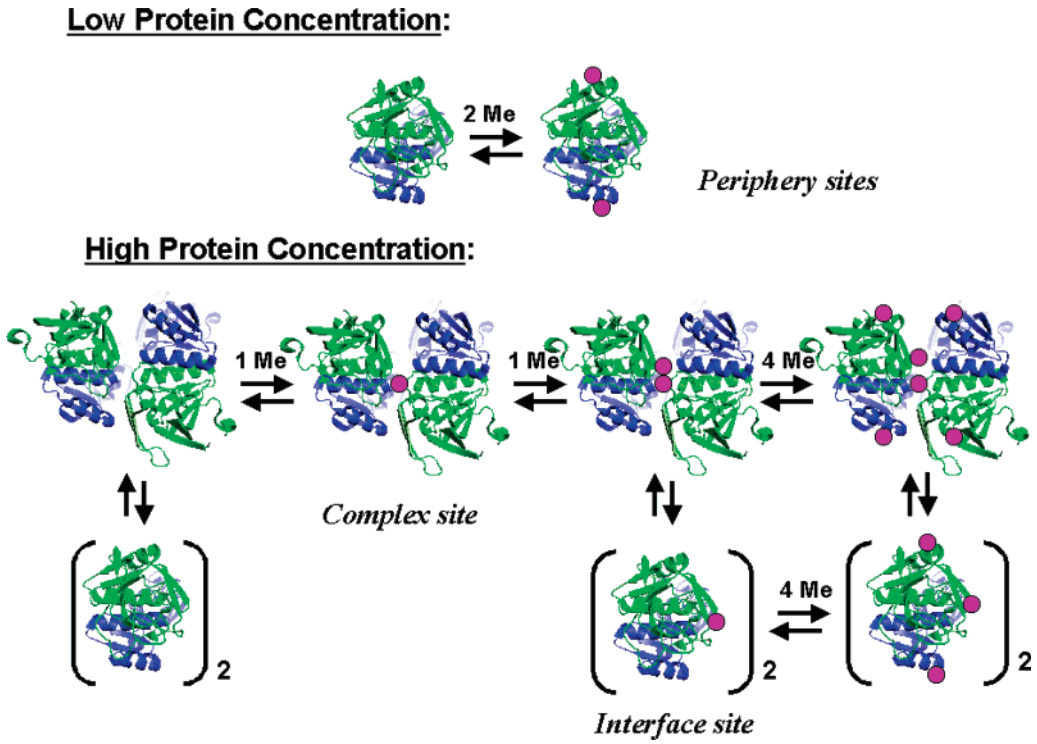

FIGURE 5: Model of metal ion interactions with the H144*UreE dimer, where ribbon diagrams of the two subunits are shown in green and blue. At low protein concentrations (<10 μM), Ni^{2+}, Cu^{2+}, and Zn^{2+} bind to periphery sites on the H144*UreE dimer that, on the basis of the Cu^{2+}-bound structure (PDB access code 1gmw), involve His-110 and His-112 on each subunit.[4] At high protein concentrations (>20 μM) one Cu^{2+} or Ni^{2+} binds initially at the complex site (four His-96 ligands) of a tetrameric species (the structure shown is from PDB code 1ear derived using *B. pasteurii* UreE), which is in equilibrium with two of the as-isolated dimers ([ ]$_2$), and then a second metal binds, giving one at each dimer interface site (two His-96 ligands per metal), and finally additional metals bind at the periphery sites of the tetramer or two of the as-isolated dimers ([ ]$_2$).

dialysis measurements, thereby providing comparable buffer- and pH-independent values.

In the case of H144*UreE, analysis of equilibrium dialysis data indicated different affinities for the two Ni^{2+} ions (*15*, *16*), while the ITC data do not distinguish the two binding events, which have a buffer- and pH-independent log *K* value of 8.8 (K_d = 1.6 nM) (Table 1). To address this discrepancy we have re-fit the equilibrium dialysis data[3] with the three binding models used to evaluate the ITC data. For previously published dialysis data (*15*), the one site model gives a good fit, although the two independent sites and two sequential sites models, which have more fit parameters, give somewhat better fits with K_1 and K_2 values that bracket the one site value. A recent set of equilibrium dialysis data obtained at pH 7.9 in 50 mM Tris and 85 mM NaCl was fit with the one site model (χ^2 = 0.048) and gives a buffer- and pH-independent log *K* value of 8.43 (K_d = 3.7 nM), in good agreement with the ITC result. Fitting these data with the two independent sites model (χ^2 = 0.051) and two sequential sites model (χ^2 = 0.051) gives log *K* (K_d) values of 8.83 (1.5 nM) and 7.97 (11 nM), and 8.53 (3.0 nM) and 8.23 (5.3 nM), respectively, but no improvement over the fit with the one site model. Thus, ITC and equilibrium dialysis results on Ni^{2+} binding to H144*UreE are in agreement that two Ni^{2+} ions bind to the dimer with similar affinities in the low nanomolar range, after buffer and proton competition have been removed.

This good agreement between the ITC and equilibrium dialysis values for Ni^{2+} binding to H144*UreE indicates that buffer- and pH-independent affinities from ITC data with other metal ions can be compared. In a trend predicted by the Irving−Williams series (*34*), the log *K* (K_d) values for Ni^{2+}, Cu^{2+}, and Zn^{2+} are 8.8 ± 0.2 (1.6 nM), 11.8 ± 0.5 (7.7 pM), and 7.1 ± 0.1 (87 nM), respectively. The large difference between the UreE affinities for Ni^{2+} and Cu^{2+} suggests that it could be more effective as a copper metallochaperone and raises questions about the Ni-selectivity of this protein. However, the relevant copper oxidation state under reducing intracellular conditions is Cu^{+} (*35*), which would have a much lower affinity than Ni^{2+} for the histidines at the UreE metal-binding sites. The average *Ka*UreE dimer affinity for the 3−4 Ni^{2+} ions that bind to its C-terminal His-rich sequences was found to be log *K* = 7.0 ± 0.2 (K_d = 82 nM), which is ~65-fold lower than that of the peripheral sites. This difference is reasonable for sites that might serve for temporary or transient Ni^{2+} storage.

Although little heat and a featureless titration profile are observed for Ni^{2+} binding to *Bp*UreE (Figure 3), the ITC data indicate a stoichiometry of ~2, which is consistent with

[3] In the course of this evaluation, we realized that certain previously published H144*UreE equilibrium dialysis data had not been fit correctly; in particular, some fits made use of total metal ion concentrations, rather than free metal ion concentrations, in the calculations, and the analysis did not take into account the buffer- and pH-dependence of binding. The corrected values are reported here and have been used in this comparison with ITC results.

[4] The ITC results cannot rule out the possibility of one metal binding to the periphery site of H144*UreE monomers at low concentration, which also gives two metals/dimer and would distinguish this low concentration stoichiometry from the high concentration stoichiometry of three metals/dimer. However, there is currently no evidence for UreE monomers in equilibrium with the dimer at low protein concentrations, and an explanation for this difference in metal binding stoichiometry is the subject of ongoing investigation.

Table 4: Buffer- and pH-Independent Thermodynamic Values[a] for Metal Ions Binding to H144*UreE, *Ka*UreE, and *Bp*UreE at 25 °C

		$\Delta G°$ (kcal/mol)	$\Delta H°$ (kcal/mol)	$\Delta S°$ (cal/mol K)
H144*UreE	Ni^{2+}	−12.0 (0.2)	−14 (2)	−8 (7)
"	Cu^{2+}	−14.7 (0.2)	−10 (4)	+15 (13)
"	Zn^{2+}	−9.6 (0.1)	−11 (2)	−4 (8)
*Ka*UreE	Ni^{2+}(1,2)	−12.0 (0.2)	−14 (2)	−8 (7)
	Ni^{2+}(3−6)	−9.5 (0.1)	−5 (3)	+17 (8)
*Bp*UreE	Ni^{2+}(1)	−10.3 (0.1)	−3 (1)	+26 (5)
	Ni^{2+}(2)	−8.5 (0.2)	0 (4)	+29 (13)

[a] The associated error is shown in parentheses.

a recent study, and the data were fit to obtain binding constants for comparison to values from equilibrium dialysis measurements in this recent study (*20*). Two factors, the low *K* value from the fit with the one site model and a comparison of the χ^2 values from the fits with different models, suggest that this protein has somewhat different affinities (K_d) for the two Ni^{2+} ions, which were found to be log $K_1 = 7.6 \pm 0.1$ (29 nM) and log $K_2 = 6.2 \pm 0.2$ (420 nM). Equilibrium dialysis data for Ni^{2+} binding to *Bp*UreE has been analyzed with three models that are similar to those used to analyze the ITC data (*20*). The one site model gave a poorer fit to the data than did two site models, and the best fit was obtained with a cooperative model that gives buffer- and pH-independent affinities (K_d) of log $K_1 = 7.78$ (17 nM) and log $K_2 = 6.52$ (300 nM) for the two Ni^{2+} ions. Thus, the Ni^{2+} affinities of *Bp*UreE determined with the two methods are in good agreement.

Thermodynamics. The thermodynamics of Ni^{2+} binding to H144*UreE, *Ka*UreE, and *Bp*UreE, as well as Cu^{2+} and Zn^{2+} binding to H144*UreE, are summarized in Table 4. The results for Ni^{2+}, Cu^{2+}, and Zn^{2+} binding to H144*UreE at low concentration reveal an enthalpically driven process with an entropic penalty for both Ni^{2+} and Zn^{2+}, but favorable changes in both enthalpy and entropy for Cu^{2+}, which contribute to its higher affinity. Although there is no UreE structure with bound Ni^{2+} ions, the X-ray structure of H91A H144*UreE with three bound Cu^{2+} ions (*21*) and the correlation between ITC data for Ni^{2+} and Cu^{2+} binding at lower and higher concentrations suggest that the two Ni^{2+} and Cu^{2+}, and presumably Zn^{2+}, ions bind at the periphery sites of the H144*UreE dimer.

Two thermodynamic factors, however, are not consistent with identical H144*UreE coordination for Ni^{2+} and Cu^{2+}. The first is the opposite sign of the entropy contribution to Ni^{2+} and Cu^{2+} binding, and the second is the magnitude of the Cu^{2+} binding enthalpy that, in comparison to those of Ni^{2+} and Zn^{2+}, is lower than predicted by the Irving−Williams series (*34*) for identical binding sites. There is spectroscopic evidence (*15*, *17*), supported by site-specific mutagenesis (*16*), for Cu^{2+} binding to Cys-79, but this is associated with Cu^{2+} binding at a significantly lower affinity (*15*) and there is no evidence for Cu^{2+} coordination to this residue in the X-ray diffraction of H91A H144*UreE crystals soaked for 2 h in 50 mM $CuSO_4$ (*21*). However, it is important to note that both spectroscopic measurements and the crystallography used samples with relatively high protein concentrations. At lower, and probably more physiologically relevant, protein concentrations (5−10 μM) the ITC data suggest that both Ni^{2+} and Cu^{2+} bind at the two periphery sites of the H144*UreE dimer. The difference between their binding thermodynamics indicates somewhat different coordination that might involve adjacent residue His-109, in addition to His-110 and His-112.

A rigorous thermodynamic analysis of metal binding to the tetramer complex or the interface site of H144*UreE was not possible due to the complexity of the calorimetric data, but the two approaches used to fit the data allow us to make some qualitative comparisons. While the sequential approach is the most accurate for the whole titration, both approaches give stability constants for the metal−tetramer complex that are somewhat greater than that of the metal bound at the interface site, particularly when the magnitude of the associated error is considered. This modest difference supports the need for a significant excess of protein to form the Cu/Ni(H144*UreE)$_4$ complex, which may explain why it has not been observed previously. Metal binding to the tetramer is generally less exothermic, particularly for Cu^{2+}, suggesting an entropic contribution to complex stability, possibly desolvation at the subunit interfaces. Metal binding to the dimer interface site, however, has a large exothermic term, suggesting that Ni^{2+} or Cu^{2+} coordination at this site is accompanied by significant favorable protein−protein interactions.

The additional Ni^{2+} ions that bind to the His-rich C-terminal sequence of *Ka*UreE do so with lower affinity and different thermodynamics than metals binding to the initial two sites. This binding is much less enthalpically favored and has a positive entropy term. The latter contribution to the free energy may be rationalized by desolvation of the 10 His residues upon binding the 1.5−2 Ni^{2+} ions (20 His residues per dimer bind 3−4 Ni^{2+} ions). However, the lower enthalpy for predominantly His coordination to the protein is a bit surprising. Since the X-ray structure of H144*UreE shows that the two C-terminal His-rich sequences would be adjacent in the dimer structure (*21*), this suggests the possibility of an interaction between them in the apoprotein that lowers the net enthalpy of Ni^{2+} coordination. With such a high local concentration of histidine residues, there may be aromatic interactions in the absence of metal, as have been noted in protein structures (*36*).

Although two Ni^{2+} ions bind to H144*UreE and *Bp*UreE, and both proteins have a relatively high affinity for these two ions, there are significant differences: (a) H144*UreE has a quantifiably higher affinity (1−2 orders of magnitude) for the two Ni^{2+} ions; (b) H144*UreE has affinities for the two Ni^{2+} ions that are not distinguishable by ITC or equilibrium dialysis, while best fits to both ITC and equilibrium dialysis data indicate a quantifiable difference between the *Bp*UreE affinities for the two Ni^{2+} ions; and (c) most importantly, Ni^{2+} binding to *Bp*UreE is predominantly an entropically driven process, distinguishing it from the entirely enthalpically favored binding of Ni^{2+} to H144*UreE. These results, which are based on a simple model of metal ions binding to protein residues (e.g., eq 5), indicate chemically different Ni^{2+} coordination to *Ka*UreE and *Bp*UreE. This difference is consistent with (a) *Bp*UreE lacking the two His residues of the periphery binding site of *Ka*UreE and (b) the recent analysis of *Bp*UreE EXAFS data that suggests a bridging ligand between the two Ni^{2+} ions, which may bind at a dinuclear site involving the two essential

His-100 residues and/or the C-terminal His-145/His-147 pairs of the *Bp*UreE dimer (*20*).

The temperature dependence of ΔH for a molecular process allows the change in heat capacity, ΔC_p, to be quantified. Since ΔC_p is also linked to the change in entropy by the thermodynamic definition, $\Delta C_p = T(\delta \Delta S/\delta T)$, a dominant contribution to ΔS, and therefore ΔC_p, in biological reactions involves changes that affect ordered water. It follows that a negative ΔC_p value indicates a decrease in the amount of ordered water molecules, while a positive value suggests the opposite effect (*37*). In the case of ligands binding to proteins, $\Delta C_p < 0$ has been associated with ligand-induced structural changes that bury hydrophobic residues and liberate solvent (*38*). This trend is also observed when the "ligand" is a metal ion. For example, there is a significant change in the structure of transferrins when they bind Fe^{3+} ions and this is associated with ΔC_p values ranging from -70 to -520 cal/(mol K) for the C and N domains in different buffers (*39*, *40*). On the other hand, Cu^{2+} binding to the three N-terminal residues of albumin, which are not observed in the X-ray structure due to disorder (*41*), is not expected to have a significant effect on the protein structure and a small positive value of ΔC_p ($+30$ cal/(mol K)) has been measured (Y. Zhang, D. E. Wilcox, unpublished results).

Analysis of ITC data for Ni^{2+} and Cu^{2+} binding to H144*UreE over the 10−37 °C temperature range indicates modest negative ΔC_p values, albeit with relatively large error bars. While this uncertainty tempers any interpretation, the relatively small negative values of -30 and -70 cal/(mol K) for Ni^{2+} and Cu^{2+}, respectively, suggest a fairly small perturbation of the UreE protein structure upon metal coordination, which is consistent with surface exposed binding sites. A small negative value of ΔC_p may even be correlated with the swiveling motion of His-112 toward His-110 upon metal binding, which is seen in the crystal structures (*21*), resulting in partial burial of hydrophobic residues and more disorder among structured waters. A small ΔC_p value is also consistent with NMR data on *Bp*UreE, which suggest that there is no major structural change upon metal coordination (*33*).

Two spectroscopically distinguishable Ni^{2+} binding sites have been reported for H144*UreE (*17*), each characterized by a pseudo-octahedral geometry consisting of O/N ligands but with different numbers of coordinating histidines. This is not inconsistent with the Ni^{2+}-binding thermodynamics, if the experimental conditions are considered. The millimolar concentration of H144*UreE used for spectroscopic measurements is well above the threshold needed to provide the three distinct binding sites indicated by ITC (Figure S3, Supporting Information). With a Ni^{2+}/dimer ratio of 1, the interface site is occupied, while the second Ni^{2+} at a ratio of 2 is distributed between the two periphery sites. Although this does not explain the different number of His ligands, under the experimental conditions there may be some coordination by His-109, as well as His-110 and His-112, at the periphery sites or some $Ni(H144*UreE)_4$, which would have four coordinating histidines.

Site-specific mutagenesis has been used to elucidate the role of certain H144*UreE residues in binding Ni^{2+} ions (*16*). The conserved and essential His-96 is not required for binding the two Ni^{2+} ions, which is consistent with their coordination to the periphery site, as inferred by the ITC results. This suggests that His-96 may be mechanistically important in metal transfer to urease apoprotein, as it does not bind Ni^{2+} in the resting Ni-loaded form of UreE at the expected low physiologically relevant protein concentrations. Both of the H110A and H112A variants have lower Ni^{2+} binding stoichiometry, as determined by equilibrium dialysis, consistent with Ni^{2+} binding to the periphery site; however, these mutants still bind 1.1 and 1.3 Ni^{2+} ions, respectively, with a quantifiable increase in affinity over the native protein. This may indicate a compensatory role by adjacent His-109 or other features of the H144*UreE dimer at low protein concentrations.

Summary. ITC data have confirmed the metal binding stoichiometry of three dimeric forms of UreE at low protein concentrations (<10 μM) and have provided new evidence that H144*UreE has additional binding sites at higher protein concentrations (>20 μM). Whether or not the higher concentrations are physiologically relevant, the additional binding sites may reflect functionally important sites that become available upon interaction of the UreE dimer with a protein complex containing urease apoprotein. These results explain some discrepancies between previous biochemical, spectroscopic, and structural results. The Ni^{2+} affinities measured by ITC agree well with those determined by equilibrium dialysis, when differences in pH and buffer competition are removed. Finally, the thermodynamics of Ni^{2+} binding to UreE from *K. aerogenes* and *B. pasteurii* have been quantified and are found to be both qualitatively and quantitatively different, with an enthalpically favored binding to *Ka*UreE, but a predominantly entropically favored binding to *Bp*UreE. This difference may be the basis for a subclassification of UreE proteins into those like *Ka*UreE with a His-rich C-terminus and enthalpically driven Ni^{2+} binding and those like *Bp*UreE that lack a His-rich C-terminus and have an entropically driven Ni^{2+} binding.

SUPPORTING INFORMATION AVAILABLE

Four figures (S1, ITC titration of H144*UreE into 20 μM Ni^{2+}; S2, ITC titration of Cu^{2+} into 12 μM H144*UreE dimer; S3, ITC titration of Ni^{2+} into 25 μM H144*UreE dimer; and S4, ITC titration of Zn^{2+} into 7.5 μM *Bp*UreE dimer) and two tables (S1, thermodynamics of metal−buffer complex formation; and S2, thermodynamic values used for temperature dependence studies). This material is available free of charge via the Internet at http://pubs.acs.org.

REFERENCES

1. O'Halloran, T. V., and Culotta, V. C. (2000) Metallochaperones, an Intracellular Shuttle Service for Metal Ions, *J. Biol. Chem. 275*, 25057−25060.
2. Quiroz, S., Kim, J. K., Mulrooney, S. B., and Hausinger, R. P. (2007) Chaperones of Nickel Metabolism, *Met. Ions Life Sci. 2*, 519−544.
3. Andrews, R. K., Blakeley, R. L., and Zerner, B. (1984) Urea and Urease, *Adv. Inorg. Biochem. 6*, 245−283.
4. Hausinger, R. P., and Karplus, P. A. (2001) Urease, in *Handbook of Metalloproteins* (Messerschmidt, A., Huber, R., Poulos, T., and Wieghardt, K., Eds.) 1st ed., pp 866−879, John Wiley & Sons, Chichester.
5. King, G. J., and Zerner, B. (1997) Jack Bean Urease: Mixed-Metal Derivatives, *Inorg. Chim. Acta 255*, 381−388.
6. Lee, M. H., Mulrooney, S. B., and Hausinger, R. P. (1990) Purification, Characterization, and In vivo Reconstitution of *Klebsiella aerogenes* Urease Apoenzyme, *J. Bacteriol. 172*, 4427−4431.

7. Park, I. S., and Hausinger, R. P. (1996) Metal Ion Interactions with Urease and UreD-Urease Apoproteins, *Biochemistry 35*, 5345−5352.
8. Jabri, E., Carr, M. B., Hausinger, R. P., and Karplus, P. A. (1995) The Crystal-Structure of Urease from *Klebsiella aerogenes*, *Science 268*, 998−1004.
9. Jabri, E., and Karplus, P. A. (1996) Structures of the Klebsiella Aerogenes Urease Apoenzyme and Two Active-Site Mutants, *Biochemistry 35*, 10616−10626.
10. Benini, S., Rypniewski, W., Wilson, K., Miletti, S., Ciurli, S., and Mangani, S. (1999) A New Proposal for Urease Mechanism Based on the Crystal Structures of the Native and Inhibited Enzyme from *Bacillus pasteurii*: Why Urea Hydrolysis Costs Two Nickels, *Structure 7*, 205−216.
11. Mulrooney, S. B., and Hausinger, R. P. (1990) Sequence of the *Klebsiella aerogenes* Urease Genes and Evidence for Accessory Proteins Facilitating Nickel Incorporation, *J. Bacteriol. 172*, 5837−5843.
12. Lee, M. H., Mulrooney, S. B., Renner, M. J., Markowitz, Y., and Hausinger, R. P. (1992) Klebsiella aerogenes Urease Gene-Cluster—Sequence of ureD and Demonstration that 4 Accessory Genes (ureD, ureE, ureF, and ureG) are Involved in Nickel Metallocenter Biosynthesis, *J. Bacteriol. 174*, 4324−4330.
13. Park, I. S., and Hausinger, R. P. (1995) Evidence for the Presence of Urease Apoprotein Complexes Containing UreD, UreF, and UreG in Cells that are Competent for in Vivo Enzyme Activation, *J. Bacteriol. 177*, 1947−1951.
14. Lee, M. H., Pankratz, H. S., Wang, S., Scott, R. A., Finnegan, M. G., Johnson, M. K., Ippolito, J. A., Christianson, D. W., and Hausinger, R. P. (1993) Purification and Characterization of *Klebsiella aerogenes* UreE Protein—a Nickel-Binding Protein that Functions in Urease Metallocenter Assembly, *Protein Sci. 2*, 1042−1052.
15. Brayman, T. G., and Hausinger, R. P. (1996) Purification, Characterization, and Functional Analysis of a Truncated *Klebsiella aerogenes* UreE Urease Accessory Protein Lacking the Histidine-Rich Carboxyl Terminus, *J. Bacteriol. 178*, 5410−5416.
16. Colpas, G. J., Brayman, T. G., Ming, L. J., and Hausinger, R. P. (1999) Identification of Metal-Binding Residues in the *Klebsiella aerogenes* Urease Nickel Metallochaperone, UreE, *Biochemistry 38*, 4078−4088.
17. Colpas, G. J., Brayman, T. G., McCracken, J., Pressler, M. A., Babcock, G. T., Ming, L. J., Colangelo, C. M., Scott, R. A., and Hausinger, R. P. (1998) Spectroscopic Characterization of Metal Binding by *Klebsiella aerogenes* UreE Urease Accessory Protein, *J. Biol. Inorg. Chem. 3*, 150−160.
18. You, J. H., Song, B. H., Kim, J. G., Lee, M. H., and Kim, S. D. (1995) Genetic Organization and Nucleotide Sequencing of the *ure* Gene-Cluster in *Bacillus pasteurii*, *Mol. Cells 5*, 359−369.
19. Ciurli, S., Safarov, N., Miletti, S., Dikiy, A., Christensen, S. K., Kornetzky, K., Bryant, D. A., Vandenberghe, I., Devreese, B., Samyn, B., Remaut, H., and Van Beeumen, J. (2002) Molecular Characterization of *Bacillus pasteurii* UreE, a Metal-Binding Chaperone for the Assembly of the Urease Active Site, *J. Biol. Inorg. Chem. 7*, 623−631.
20. Stola, M., Musiani, F., Mangani, S., Turano, P., Safarov, N., Zambelli, B., and Ciurli, S. (2006) The Nickel Site of *Bacillus pasteurii* UreE, a Urease Metallo-Chaperone, as Revealed by Metal-Binding Studies and X-Ray Absorption Spectroscopy, *Biochemistry 45*, 6495−6509.
21. Song, H. K., Mulrooney, S. B., Huber, R., and Hausinger, R. P. (2001) Crystal Structure of *Klebsiella aerogenes* UreE, a Nickel-Binding Metallochaperone for Urease Activation, *J. Biol. Chem. 276*, 49359−49364.
22. Remaut, H., Safarov, N., Ciurli, S., and Van Beeumen, J. (2001) Structural Basis for Ni^{2+} Transport and Assembly of the Urease Active Site by the Metallochaperone UreE from *Bacillus pasteurii*, *J. Biol. Chem. 276*, 49365−49370.
23. Kim, J. K., Mulrooney, S. B., and Hausinger, R. P. (2005) Biosynthesis of Active *Bacillus subtilis* Urease in the Absence of Known Urease Accessory Proteins, *J. Bacteriol. 187*, 7150−7154.
24. *Peptide Properties Calculator*. http://www.basic.northwestern.edu/biotools/proteincalc.html
25. Zhang, Y., Akilesh, S., and Wilcox, D. E. (2000) Isothermal Titration Calorimetry Measurements of Ni(II) and Cu(II) Binding to His, GlyGlyHis, HisGlyHis, and Bovine Serum Albumin: A Critical Evaluation, *Inorg. Chem. 39*, 3057−3064.
26. MicroCal. (2002) *VP-ITC MicroCalorimeter User's Manual*, Northampton, MA.
27. Grossoehme, N. E., Akilesh, S., Guerinot, M. L., and Wilcox, D. E. (2006) Metal-Binding Thermodynamics of the Histidine-Rich Sequence from the Metal-Transport Protein IRT1 of *Arabidopsis thaliana*, *Inorg. Chem. 45*, 8500−8508.
28. Doyle, M. L., Louie, G., Dal, Monte, P. R., and Sokoloski, T. D. (1995) Tight Binding Affinities Determined from Thermodynamic Linkage to Protons by Titration Calorimetry, *Methods Enzymol. 259*, 183−194.
29. NIST Standard Reference Database 46 (2003).
30. Nakon, R., and Krishnamoorthy, C. (1983) Free-Metal Ion Depletion by "Good's" Buffers, *Science 221*, 749−750.
31. Wiseman, T., Williston, S., Brandts, J. F., and Lin, L. (1989) Rapid Measurement of Binding Constants and Heats of Binding using a New Titration Calorimeter, *Anal. Biochem. 179*, 131−137.
32. Moncrief, M. B. C., and Hausinger, R. P. (1996) Nickel Incorporation into Urease, in *Mechanisms of Metallocenter Assembly* (Hausinger, R. P., Eichhorn, G. L., and Marzilli, L. G., Eds.) pp 151−171, Elsevier, New York.
33. Won, H. S., Lee, Y. H., Kim, J. H., Shin, I. S., Lee, M. H., and Lee, B. J. (2004) Structural Characterization of the Nickel-Binding Properties of *Bacillus pasteurii* Urease Accessory Protein (Ure)E in Solution, *J. Biol. Chem. 279*, 17466−17472.
34. Irving, H., and Williams, R. J. P. (1948) Order of Stability of Metal Complexes, *Nature 162*, 746−747.
35. Huffman, D. L., and O'Halloran, T. V. (2001) Function, Structure, and Mechanism of Intracellular Copper Trafficking Proteins, *Annu. Rev. Biochem. 70*, 677−701.
36. Wang, L. J., Sun, N., Terzyan, S., Zhang, X. J., and Benson, D. R. (2006) Histidine/tryptophan Pi-Stacking Interaction Stabilizes the Heme-Independent Folding Core of Microsomal Apocytochrome b_5 Relative to that of Mitochondrial Apocytochrome b_5, *Biochemistry 45*, 13750−13759.
37. Sturtevant, J. M. (1977) Heat-Capacity and Entropy Changes in Processes Involving Proteins, *Proc. Natl. Acad. Sci. U.S.A. 74*, 2236−2240.
38. Brandts, J. F. (1964) Thermodynamics of Protein Denaturation. II. Model of Reversible Denaturation and Interpretations regarding Stability of Chymotrypsinogen, *J. Am. Chem. Soc. 86*, 4302.
39. Lin, L. N., Mason, A. B., Woodworth, R. C., and Brandts, J. F. (1991) Calorimetric Studies of the Binding of Ferric Ions to Ovotransferrin and Interactions between Binding-Sites, *Biochemistry 30*, 11660−11669.
40. Lin, L. N., Mason, A. B., Woodworth, R. C., and Brandts, J. F. (1993) Calorimetric Studies of the Binding of Ferric Ions to Human Serum Transferrin, *Biochemistry 32*, 9398−9406.
41. He, X. M., and Carter, D. C. (1992) Atomic Structure and Chemistry of Human Serum Albumin, *Nature 358*, 209−215.

BI700171V